

1 **Morphogenetic and functional analysis of plant organs with sub-cellular** 2 **resolutions.**

3 **Running title: Quantitative plant cell biology *in situ*.**

4 **Abstract**

5 A shortfall of precise plant phenotyping methods at subcellular resolution limits our ability to dissect
6 the genotype-environment interactions that are critical for understanding plant adaptation to different
7 types of stresses and for linking genes with their function, expression, and localization. Here, we
8 describe an effective, high-resolution phenotyping platform that allows the detection of tissues, cell
9 files, and cell shapes, as well as protein localization, chromatin organization, cell cycle kinetics, cell
10 polarity, and protein-protein interactions at subcellular resolution. The platform does not require
11 endogenous markers and is plant-species independent. The platform has been successfully used for the
12 analysis of diverse organs in several plant species, including grasses. Application of the platform
13 requires minimal time and experience from researchers and can be completed in 3 to 4 working days
14 (including complete data extraction for each cell). The method requires a high-resolution microscope
15 and state-of-the-art computer. We present the results of platform applications in diverse developmental
16 contexts. The platform is free and open source, with a user-friendly graphical interface.

- 17 • Key words: Phenotyping, 3D imaging; segmentation; cell cycle, gene expression, epigenetics.
- 18 • Abbreviations: iRoCS- internal root coordinate system.

19

20 **Introduction.**

21 A large-scale quantitative study of cell shape and cell functionality in a multicellular organ entails an
22 accurate estimation of the quantitative three-dimensional geometry and functions of each cell in that
23 organ (Bassel, G. W., 2019). State-of-the-art confocal and other advanced microscopes with high-
24 resolution volumetric image acquisition allow researchers to scan 3-D images of the cell boundary,
25 chromatin, cell cycle events, and protein localizations for almost all plant organs (Rowland & Nickless,
26 2000). The volume, spatial position, orientation, and polarity of cells comprising an organ are important
27 phenotyping traits, as they can characterize mutant phenotypes or gene-editing effects under different
28 environmental conditions.

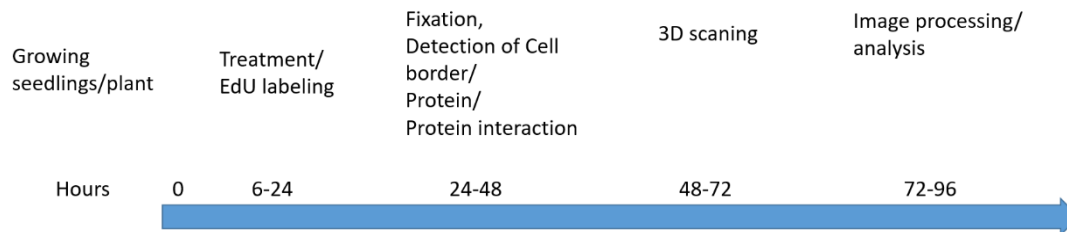
29 Recently developed methods enable precise segmentation based on cell border labeling (Liu et al., 2013,
30 2014). This approach, combined with the detection of nuclei and cell cycle events (Schulz et al., 2006;
31 Pasternak et al., 2017), allows a simultaneous analysis of cell geometry, cell cycle duration, and
32 geometry of organelles. Cell positions within organs are defined using an internal organ coordinate
33 system based on the position of the organ tip (e.g., the quiescent center [QC] in the root). Cell boundary
34 labeling facilitates the integration of multiple cell types into organ atlases with a precise description of

35 cellular neighborhoods. One recently developed technique now directs quantitative protein level
36 analysis (Omelyanchuk et al., 2016) and localization and quantification of the protein complex through
37 Proximity Ligation Assay (PLA) (Pasternak et al., 2018; Teale et al., 2021). All these approaches,
38 including the necessary protocols for whole-mount labeling, image scanning, processing, layer
39 identification, and analysis, have been integrated into the Deep-Resolution Plant Phenotyping Platform
40 (DRPPP), a deep pipeline for volumetric segmentation and analysis of the geometry of plant tissue and
41 the detection and quantitative analysis of cell volume, cell cycle events, chromatin status, gene
42 expression and protein complex at cell-level resolution. The main advantage of the DRPPP is that it
43 provides simultaneous analysis and tracking of all cells in an organ in the context of their positions
44 within that organ. The platform requires no endogenous markers; hence, it can be applied to diverse
45 plant species.

46 **Overview on the pipeline.**

47 The pipeline includes growing plants *in vitro* or in soil, incubation of plant tissues with 5-ethynyl-2'-
48 deoxyuridine (EdU) for cell cycle kinetics or other chemicals according to the task, tissue fixation,
49 labeling, scanning, and image processing.

50



51

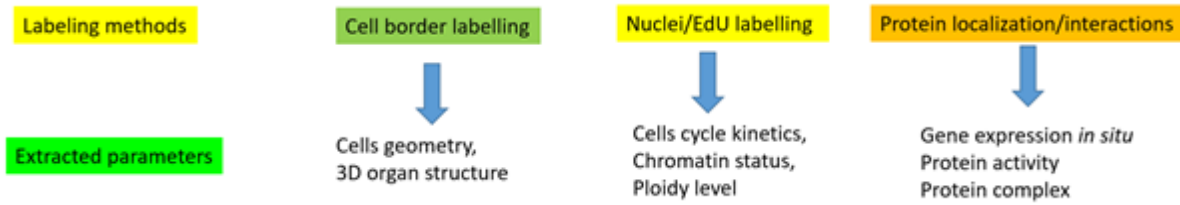
52 **Figure 1.** Pipeline step-by-step protocol with timing (in hours). The whole procedure, from treatment
53 to full extraction of the data, requires less than 96 hours.

54

55 **Labeling methods and parameters extracted.**

56 The platform includes four different tissue labeling options or their combinations: cell border labeling,
57 nucleus labeling (including EdU labeling for cell cycle kinetics), protein localization, and protein
58 complex detection. All four options can be combined to study cell geometry/cell cycle/gene expression
59 simultaneously. Since the quality of labeling is crucial for further analysis, we will describe the
60 procedure in detail in the next parts. Acquisition of the required very high-quality images is quite
61 challenging; therefore, we describe the most important aspects in detail and give protocols in the
62 upcoming sections.

63



64

65 **Figure 2.** Labeling options.

66

67 **Live and fixed tissue samples.**

68 The analysis of whole organs at sub-cellular resolution requires the recording of multiple tiles (typically
69 3–5), with a depth-dependent dynamic adaption of the recording parameters. Thus, living objects
70 (especially roots) are difficult to label and high-quality images are difficult to produce because of the
71 rapid growth and movement of the objects, although the pipeline does not preclude live imaging. High-
72 quality analyses can only be performed on fixed tissues.

73

74 **Cell boundary detection.**

75 Cell boundaries in plants can be detected based on labeling of the cell wall or plasma membrane. One
76 condition necessary for successful boundary detection by the software is an equal intensity of the
77 boundary of each cell. For this reason, simple cellulose labeling is not suitable for boundary detection
78 because of the variations in the cell wall thickness and various other cell wall properties within an organ.
79 We optimized cell wall labeling by partial digestion of the cell wall to create an almost equal signal
80 intensity for all cell layers after calcofluor white labeling. This labeling can be combined with nucleus
81 detection and gene expression analysis by immunolocalization or PLA assays. This option is especially
82 suitable for the leaves because of their equal cell wall thicknesses compared with root cells.

83 A second option is to label polysaccharides after normalization of ketone-bound digestion (so-called
84 pseudo-Schiff reagent labeling) (Pearse, 1968). However, this procedure is conducted at pH 1.4 and
85 cannot be combined with any other labeling.

86 An alternative to cell wall labeling is plasma membrane labelling, which can greatly improve the
87 evenness of the cell boundaries. The use of FM™ 4-64FX, a fixable analog of the FM™ 4-64 membrane
88 stain, gives a satisfactory segmentation quality. However, it does not allow us to combine this labeling
89 successfully with DAPI or immunostaining used for protein expression and localization. A more
90 vigorous fixation procedure using a high Triton-X100 concentration punctures the membrane lipid
91 bilayers that preclude a segmentation step.

92 We have been able to successfully combine triple labeling using calcofluor white for cell boundaries,
93 antibodies for protein localization, and propidium iodide for nucleus labeling. Another possibility is
94 to use DAPI for nuclear labeling, as this also allows the detection of cell position in the organs, although
95 it does not allow cell geometry detection.

96

97 **Mounting.**

98 A 3D scan requires full organ integrity, so a mounting spacer equal to or larger than the organ thickness
99 must be used. For Arabidopsis roots, a 120 μm spacer is sufficient. However, bigger roots, such as
100 tobacco, require a 250 μm spacer.

101

102 **Scanning procedure.**

103 Proper image analysis requires equal signal intensity through all organs. However, it is very difficult to
104 achieve in thick objects because of the samples' optical density. Equal signal intensity can be improved
105 in two ways: 1. By dynamically regulated scanning through gradual changes in detector gain, laser
106 power, averaging signal to keep signal-to-noise ratio at a similar level along the sample; 2. By the use
107 of double-sided scanning. The second way is more challenging and can be applied to the samples with
108 a thickness greater than 250 μm .

109 **Software for image analysis.**

110 The intrinsic root coordinate system (iRoCS) Toolbox was used for image analysis (Schmidt et al.,
111 2014). This software allows extraction of cell geometry and analysis of cell cycle kinetics, gene
112 expression, and protein complexes.

113

114 **Limitations of the platform.**

115 The platform can be applied to most plant organs. However, thick organs (more than 500 μm thickness)
116 may require longitudinal sectioning before processing/scanning.

117

118 **Materials and methods.**

119 Detailed protocols for the image processing and analysis is in Pasternak T. et al., 2021a.

120 <https://protocols.io/view/deep-resolution-plant-phenotyping-platform-descrip-brsdm6a6.pdf>

121 **Reagents.**

122 All reagents were described in detail previously (Pasternak et al., 2015; 2017; 2018).

123

124 **Microscope.**

125 The confocal or other microscope must provide 3D image scanning at high resolution. For thick objects,
126 we recommend using a 2-photon microscope.

127

128 **Computer.**

129 The software requires a computer with a minimal RAM size 8 (16) GB (64 GB is recommended for
130 large images with high-resolution segmentation).

131

132 **Plant material preparation and labelling.**

133 Plants of *Arabidopsis thaliana*, *Nicotiana tabacum*, *Setaria italica*, and *Lycopersicon esculentum* have
134 been used. All procedures for plant cultivation, fixation, treatments, and imaging were described
135 previously (Pasternak et al., 2015; 2017; 2020). The specific differences from the previously published
136 protocols are presented below.

137

138 **Cell boundary labeling.**

139 Our cell boundary labeling protocol is based on the binding of propidium iodide to de-ketone cell
140 wall polysaccharides at low pH (1.4) in the presence of sulfur. Although the basic protocol has been
141 described previously (Truernit et al., 2008), significant modifications are required to adapt the protocol
142 for 3D scanning and analysis. One limitation is that the original fixation in acetic acid leads to significant
143 tissue maceration and often damages the softer mature plant parts. For this reason, we recommend
144 fixation with formaldehyde in MTSB buffer at pH 7 before labeling. The de-ketone level (time of
145 periodic acid treatment) is another crucial parameter. For *Arabidopsis* roots, a 30 min de-ketone
146 in 1% periodic acid partially punctured the cell walls, especially in the mature parts. We recommend
147 reducing the de-ketone time to 15–20 minutes. The mounting procedure is another crucial step. As
148 already mentioned, the spacer should have a similar thickness to the object. A thick object can be
149 scanned using double-sided scanning by mounting the samples between 2 coverslips: a 24 × 60 mm size
150 as a base and a 24 × 32 mm size as a cover. This adjustment allows the object to be scanned from both
151 sides to avoid a low signal-to-noise ratio in the deeper parts.

152

153 **Scanning procedure.**

154 **Note:** Always adjust the immersion medium and embedding medium to the average refractive index of
155 the sample for optimum image quality, especially when conducting deep optical sectioning.

156 A confocal laser scanning microscope with at least four lasers (2P, 488, 543/561, and 633) is required.
157 We recommend the following objectives: ×25 for cell geometry with glycerol immersion and ×40 or
158 ×63 for gene expression, cell cycle, and chromatin structure analysis.

159 Scanning should be performed with at least 1024 × 1024 pixels per frame at 16 bits and with the
160 amplifier offset close to zero to avoid underexposed image regions. Z-stack corrections are highly
161 recommended to obtain a reasonable signal-to-noise ratio throughout the stack, while avoiding over-
162 exposure. To increase the image quality in the deeper parts, increase the average numbers or reduce the
163 scanning speed in this region. The choice of objective depends on the type of analysis: for cell volumetric
164 analysis ×25 or ×40 objective with immersion correction should be used. For gene expression analysis,
165 cell cycle analysis, and chromatin structure, the minimum is ×40, but ×63 objective is better.

166

167 **Data extraction/presentation.**

168 After data extraction, each cell/nucleus has three basic coordinates: the distance from the QC, the radial
169 distance, and the radians (unrolled organ). We suggest using a graphical presentation of an unrolled root,

170 e.g., radians on the x-axis and distance from the QC as the y-axis. The volume can be embedded as a
171 third set of coordinates for the cells as well as for nuclei.

172

173 **Statistical analysis.**

174 The platform allows extraction of all parameters from at least 5000 cells from Arabidopsis and 30,000
175 cells for large roots (e.g., tobacco, tomato, millet). The most commonly used method involves analysis
176 of a maximum of 100 cells per root. The platform allows the collection of more detailed information,
177 thereby providing a deeper insight into developmental processes as well as a better understanding of
178 plant responses to environmental stimuli.

179 **CASE RESULTS**

180 Here, we have demonstrated the application of the platform for diverse plant organs and species.

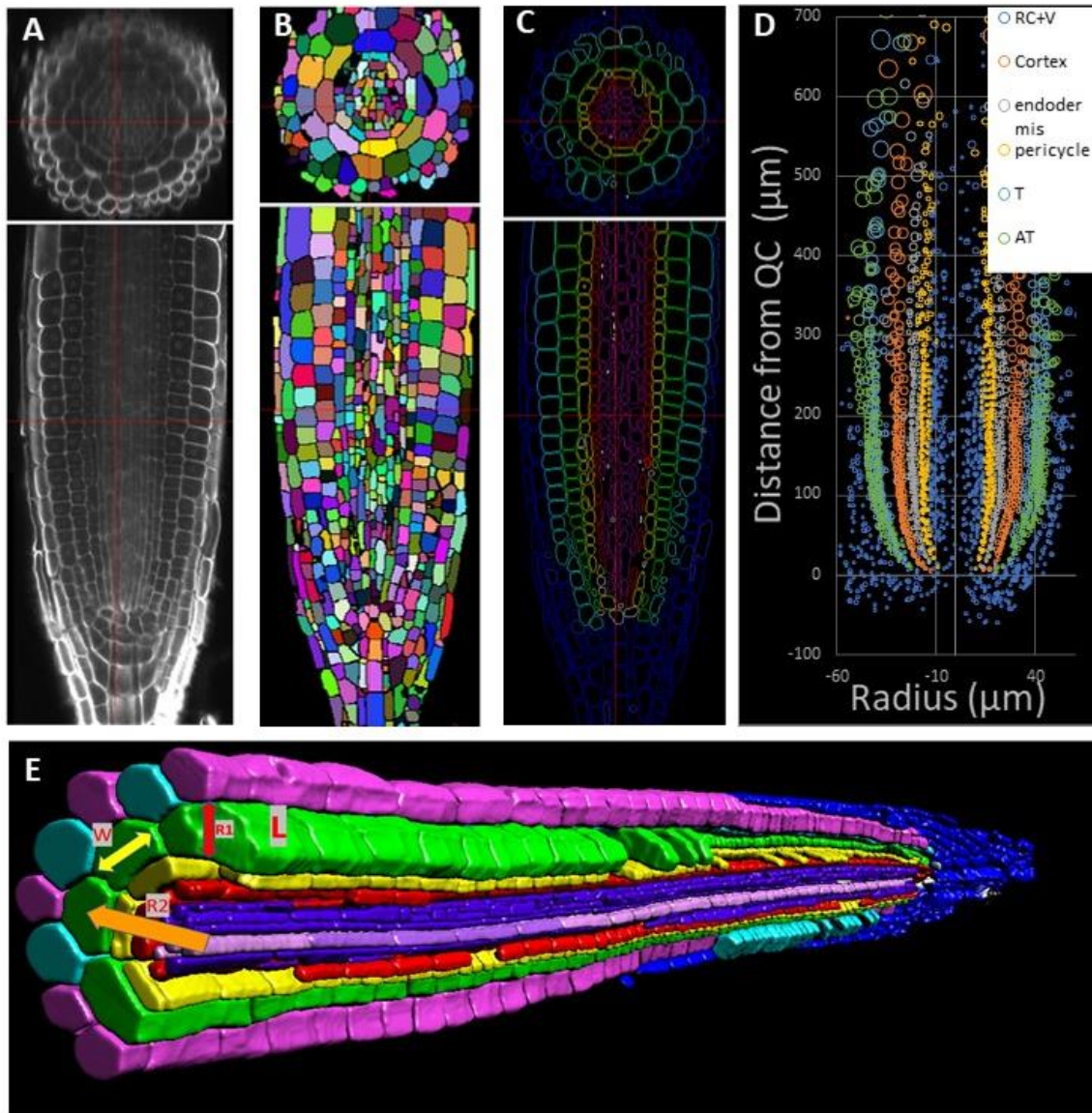
181 We applied the platform for two tasks: geometrical analysis (geometry of each cell) and functional
182 analysis, when cell function (chromatin organization, cell cycle, protein location and protein proximity)
183 were analyzed.

184

185 **I. Volumetric plant organ analysis.**

186 The most straightforward platform application is quantitative analysis of Arabidopsis root apical
187 meristem geometry with 3D resolution. This analysis includes the evaluation of cell elongation and cell
188 volume in each cell continuity. The whole pipeline is presented in Figure 3. The simple cylindrical root
189 structure is amenable to application of the root coordinate system, which in turn, allows the extraction
190 of the distance from the QC, the radial distance, and the angle.

191

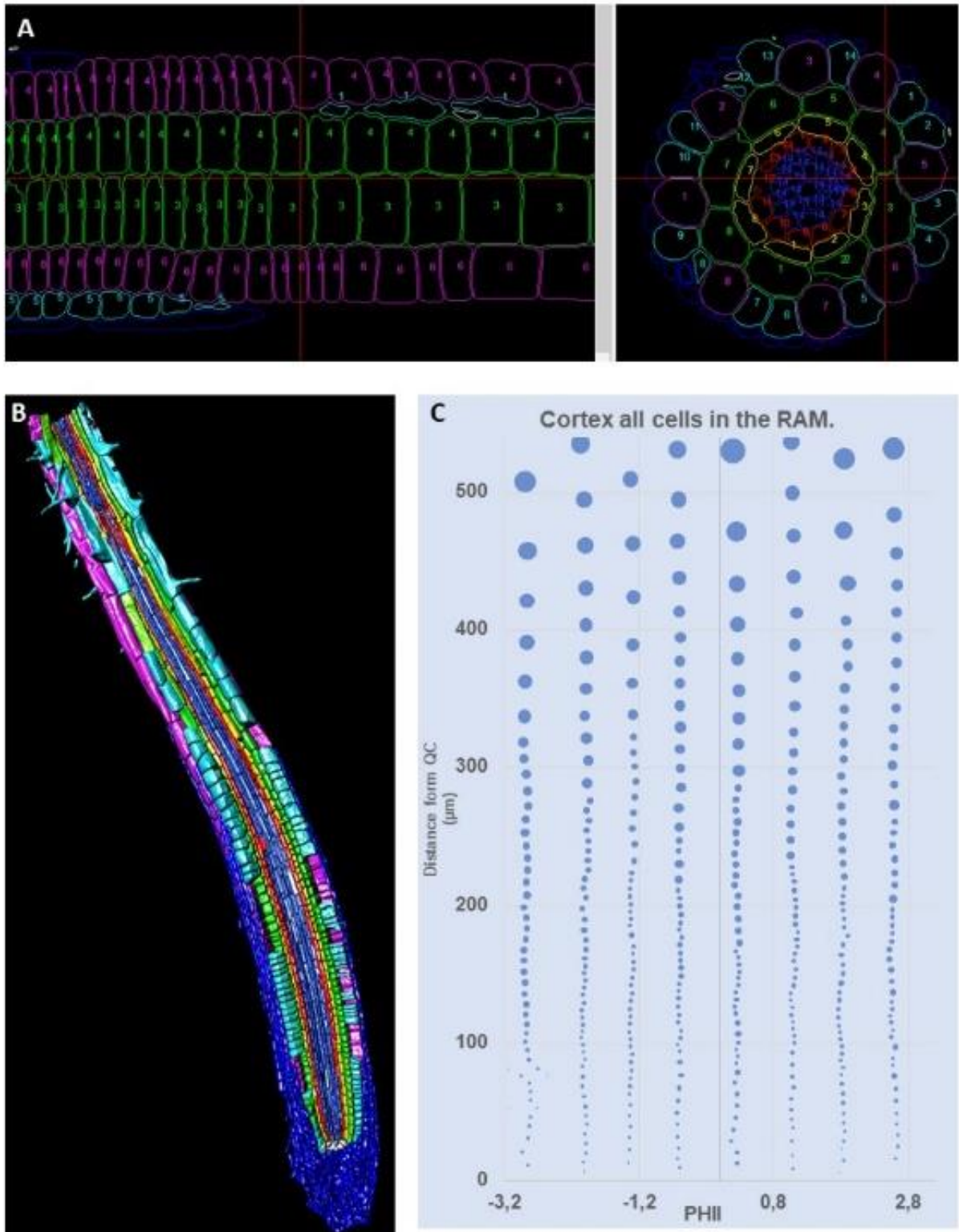


192

193

194 **Figure 3.** Graphical presentation of the pipeline for the example of the Arabidopsis root apical meristem
 195 (RAM). (a) - input image; (b) - segmentation; (c) - layers; (d) - volumetric analysis (circle size
 196 proportional to the volume); (e) - parameters extracted for the root cells all cell layers, the detailed
 197 structure of xylem/phloem, trichoblast/atrichoblast, root asymmetry in the cortex xylem and phloem
 198 poles. L - cell length; W - cell width; R1 - cell radial size; R2 - distance from the axis; R3 - radians; V -
 199 cell volume. All parameters are from all 3000 cells in the RAM and the elongation zone until full
 200 maturity, including root hairs.

201 We have also looked at the structure of the outer cell layers because the characterization of these layers
 202 provides insight into specific physiological responses. Specifically, (i) cortex length has been used for
 203 estimation of root proximal apical meristem length (Hacham et al., 2011); (ii) cell cycle kinetics in the
 204 epidermis has been used for estimation of cell cycle kinetics by the “kinematic method.”



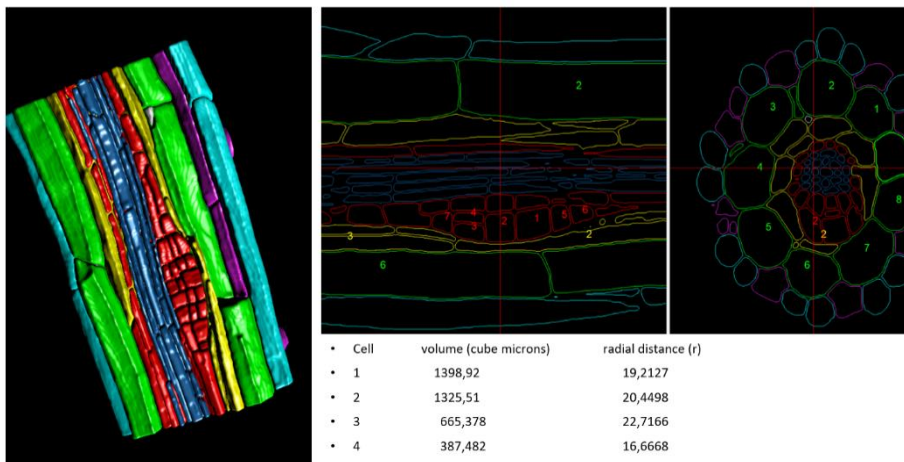
205
 206 **Figure 4.** Extraction of geometrical data from the segmented root. (a) - yz and xy views of the root with
 207 layers labeled and cell file numbers. Root caps- dark-blue; Trichoblasts (T) - magenta; Atrichoblasts
 208 (AT) - blue; cortex (C) - green; endodermis - yellow; pericycle - red; vasculature - dark blue. (b) – 3D-
 209 rendering; (c) – unrolled cortex layers.
 210
 211

212 The root waving phenomena is causally related to unequal cell elongation/expansion in the outer cell
 213 layers (cortex/epidermis) (Thompson, M. V., & Holbrook, N. M., 2004), and requires a detailed
 214 characterization of the cells in cell files for understanding of the waving mechanism of root growth.
 215 Figures 3 and 4 (a) show that the epidermis consists of 8 trichoblast (T) layers (which produce root hairs)
 216 and 14 atrichoblast (AT) layers (which usually do not produce root hairs). Interestingly, the distribution
 217 of AT is clearly asymmetric, with 1 layer (2 cases) or 2 layers (6 cases) of AT cells between the T. This
 218 led to an unequal angle between the T and cortex cell files. Figure 4 (a) shows a segmented root with
 219 numbers of each continuity and coordinate system. Figure 3 (b) shows a 3D rendering and Figure 3 (c)
 220 shows an “unrolled” root. The asymmetry in the epidermis related to the presence of 2 or 1 AT layers
 221 between the T leads to asymmetry of the cortex cells, where the cortex cells touching one AT layer have
 222 a smaller size.

223

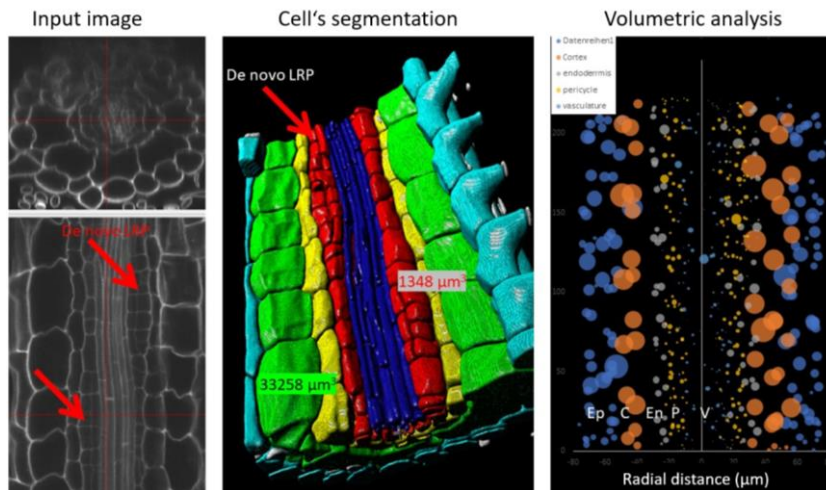
224 **Quantitative analysis of lateral organs.**

225 The lateral roots aid in anchoring the plant to the soil, while increasing water and nutrient uptake. In
 226 addition, lateral roots increase the surface area of the plant root system. Therefore, we obtained a full
 227 view of root system architecture (RSA) by testing the possibility of quantifying the kinetics of lateral
 228 root development in Arabidopsis in both natural and auxin-induced lateral root primordia (Figure S1
 229 and S2). Here, the main advantage of the platform is that it enables researchers to see the changes in all
 230 cell files, which means that it can quantify the position of a lateral root on the plant body, the position
 231 of the founder cell, and any divergence in cell volume and orientation during lateral root formation from
 232 stage I to stage VIII.



233

234 **Supplementary Figure 1.** Lateral root was segmented, layers were labeled, and quantitative data were
 235 extracted. The cell volumes of 4 cells are shown as an example. The pericycle/lateral root is indicated
 236 in red.



237

238 **Supplementary Figure 2.** *De novo* auxin-induced lateral root primordia (LRP) in the early mature zone
 239 with inhibition of cell elongation.

240

241 **Analysis of diverse plant species.**

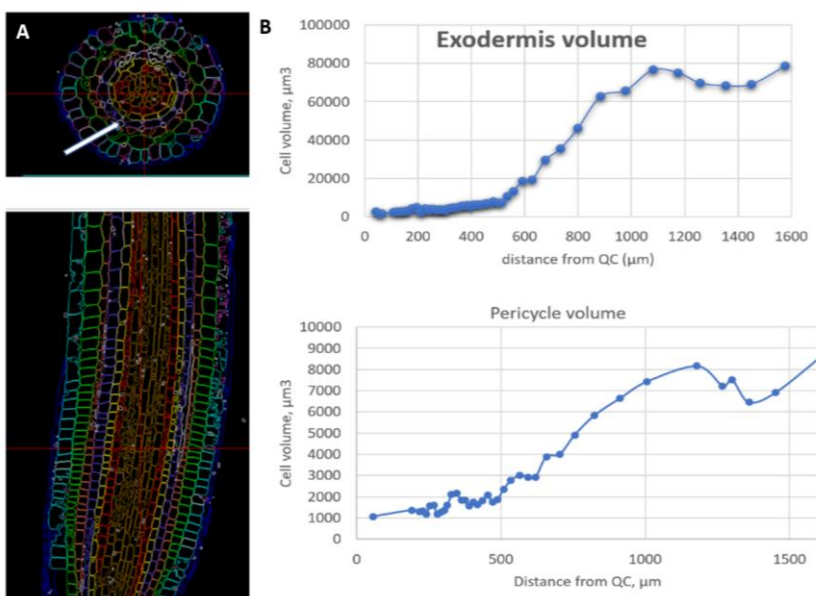
242 In addition to Arabidopsis roots, we tested applications of the protocol to larger species containing more
 243 cortex layers (tomato and tobacco) or more complicated inner cell layers (C4 plants with different
 244 xylem/phloem structure).

245

246 **Protocol application for the thick roots.**

247 The protocol allows quantitative analysis of roots of tobacco and millet with root diameters up to 300
 248 μm . These roots contain up to 4 cortex layers, so they are quite similar to the inner layers of Arabidopsis
 249 or other C3 plants, but they are completely different from C4 roots (Figure 5, 6).

250



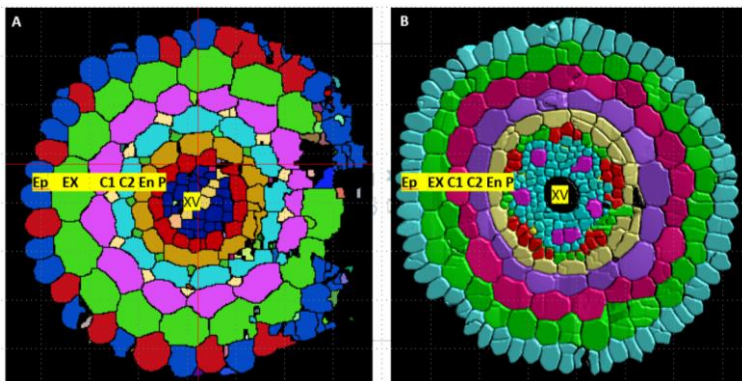
251

252

253 **Figure 5.** Tobacco root analysis. (a) Segmented and assigned tobacco root. Aerenchyma “holes”
254 occurring between cortex 2 and cortex 3 and between cortex 3 and the endodermis are indicated by white
255 arrows. (b) Evolution of the cell volume of the exodermis and pericycle along the axis. Note the 10
256 tenfold differences in the volume scale bars between the exodermis and pericycle.

257

258 As a further possible application, we compared the root structures of dicotyledonous and
259 monocotyledonous plants (tobacco and foxtail millet, as model objects for both clades). Both species
260 have a very similar outer layers structure (epidermis-exodermis, two cortex layers, and one endodermis
261 layer), but very significant differences in the inner cell layers: monocot roots are characterized by 5–6
262 large metaxylem vessels and one central cylinder (Figure 6). In the case of millet, a quantitative analysis
263 of 30000 cells up to 1.2 mm from the tip was possible.



264

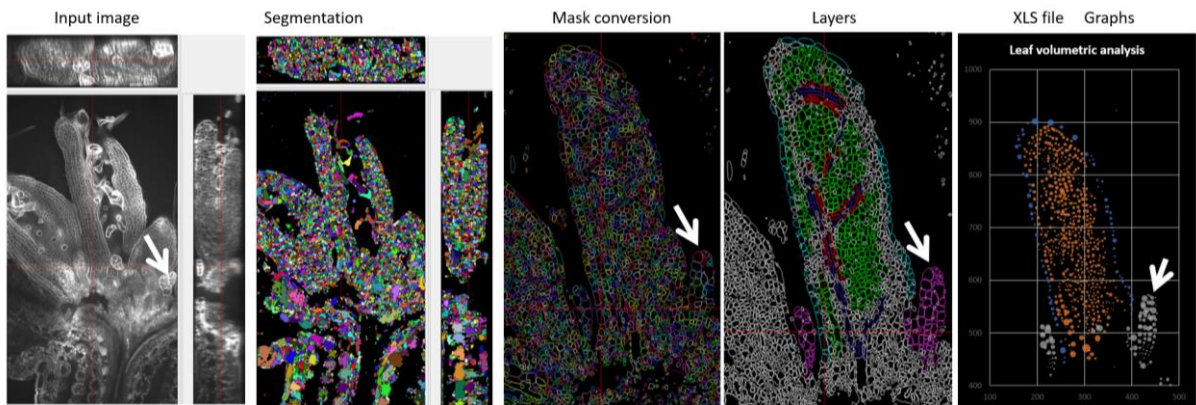
265 **Figure 6.** XY cross-section from 3D images of tobacco (A) and foxtail millet (B).

266 Ep- epidermis; Ex- exodermis; C1, C2- cortex 1 and 2; En- endodermis; P- pericycle; XV- xylem vessel.
267 Both roots were quantitatively analysed, including the volume of the central and side-xylem vessels, and
268 the asymmetric cell position.

269 **Analysis of the geometry of the aboveground part of the plants.**

270 Investigation of the cell geometry dynamics, and especially surface expansion, that accompany leaf
271 primordium formation, can be one target of DRPPP. We can quantify all the geometrical parameters of
272 each cell at all stages of leaf development and process up to 10 leaves simultaneously (68,000 cells in 7
273 to 8 day-old seedlings) with characterization of the cell position in the leaf, the shoot apical meristem
274 (SAM) structure, and the trichome and stipule volumes.

275 The platform performs an automatic extraction of all phenotypic traits for an individual leaf and an
276 individual cell in a 3D model. The most important parameters are the leaf area, the location and density
277 of the stomata cells, the volume and surface area of the mesophyll cells, and the detailed structure of the
278 vascular tissue. Simultaneous analysis of leaves of different ages (as shown in the example) allows
279 observation of structural changes during leaf development. In conclusion, polysaccharide labeling
280 allows investigation of quantitative plant organ geometry and provides equal labeling intensity to all cell
281 files, independent of the cellulose content in the cell walls.



284 **Figure 7.** Example of geometric analysis of a 7–8-day-old Arabidopsis shoot. The shoot was segmented,
 285 converted to a mask, and the features of 68,000 cells were extracted and analyzed. One leaf is shown as
 286 an example. The bubble size indicates the volume. Stipule differentiation with increasing volume is
 287 visible (yellow arrow).

288 These data can be used to prepare a plant organ zonation model with the cell division position,
 289 endocycle, and cell differentiation for each cell layer in all plant organs, while also defining the boundary
 290 zone between each.

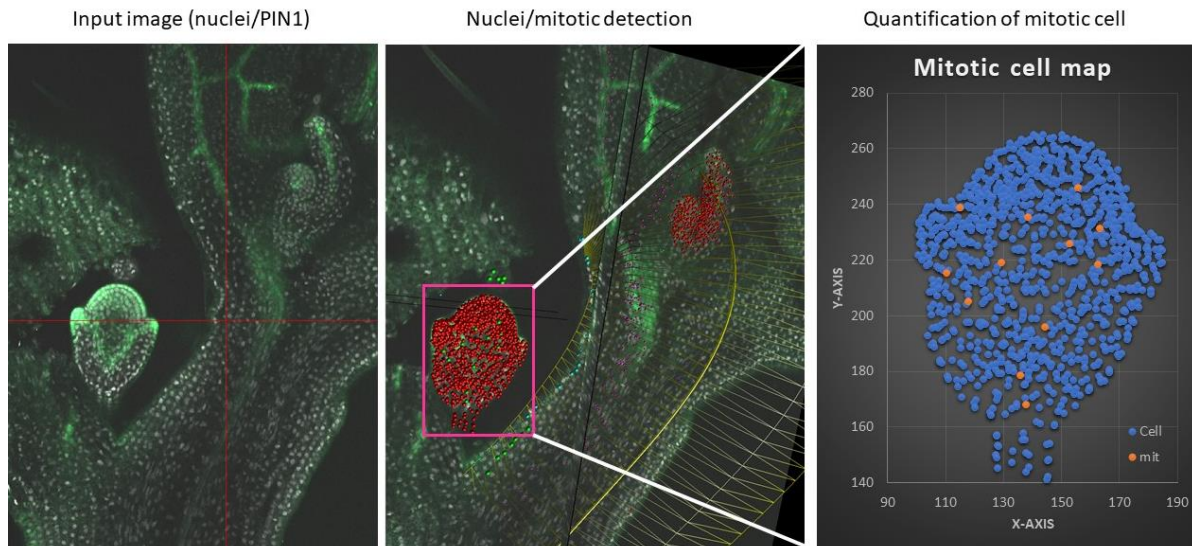
291

292 II. Functional plant organ analysis based on nuclear labeling.

293 In addition to cell border labeling, the platform also allows automatic detection of the nuclei, which in
 294 reflect position of each cell and the cell cycle status. When used in combination with EdU labeling, it
 295 allows mapping of DNA replication events as well.

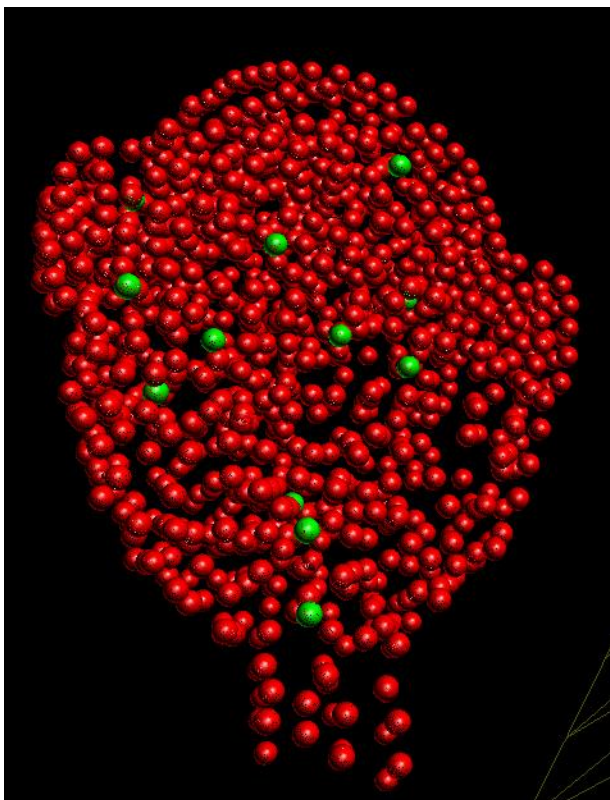
296

297 **Cell cycle analysis.** The most straightforward demonstration of the platform is a quantitative analysis
 298 of Arabidopsis root apical meristem for cell cycle activities with 3D resolution. Two key cell cycle
 299 transitions have been detected: DNA replication (after a 90 min EdU incubation) and mitosis (after a 90
 300 min colchicine incubation). Mapping of these events serves as the basis of functional root zonation: the
 301 border of the proliferation zone is the mean position of the last mitosis event in the corresponding cell
 302 file, while the border of the transition zone is defined as the starting point of rapid cell elongation and
 303 DNA reduplication. The platform can also be applied to investigate the cell cycle distribution and gene
 304 expression in the floral tissues (Supplemental Figure 3 and 4).



305

306 Figure S3. Quantitative analysis of the flowers development.



307

308 Figure S4. Details of the flower meristem.

309 **Analysis of the cell cycle kinetics.**

310 The cell cycle progression in the root apical meristem is crucial in regulating root growth and
 311 development.

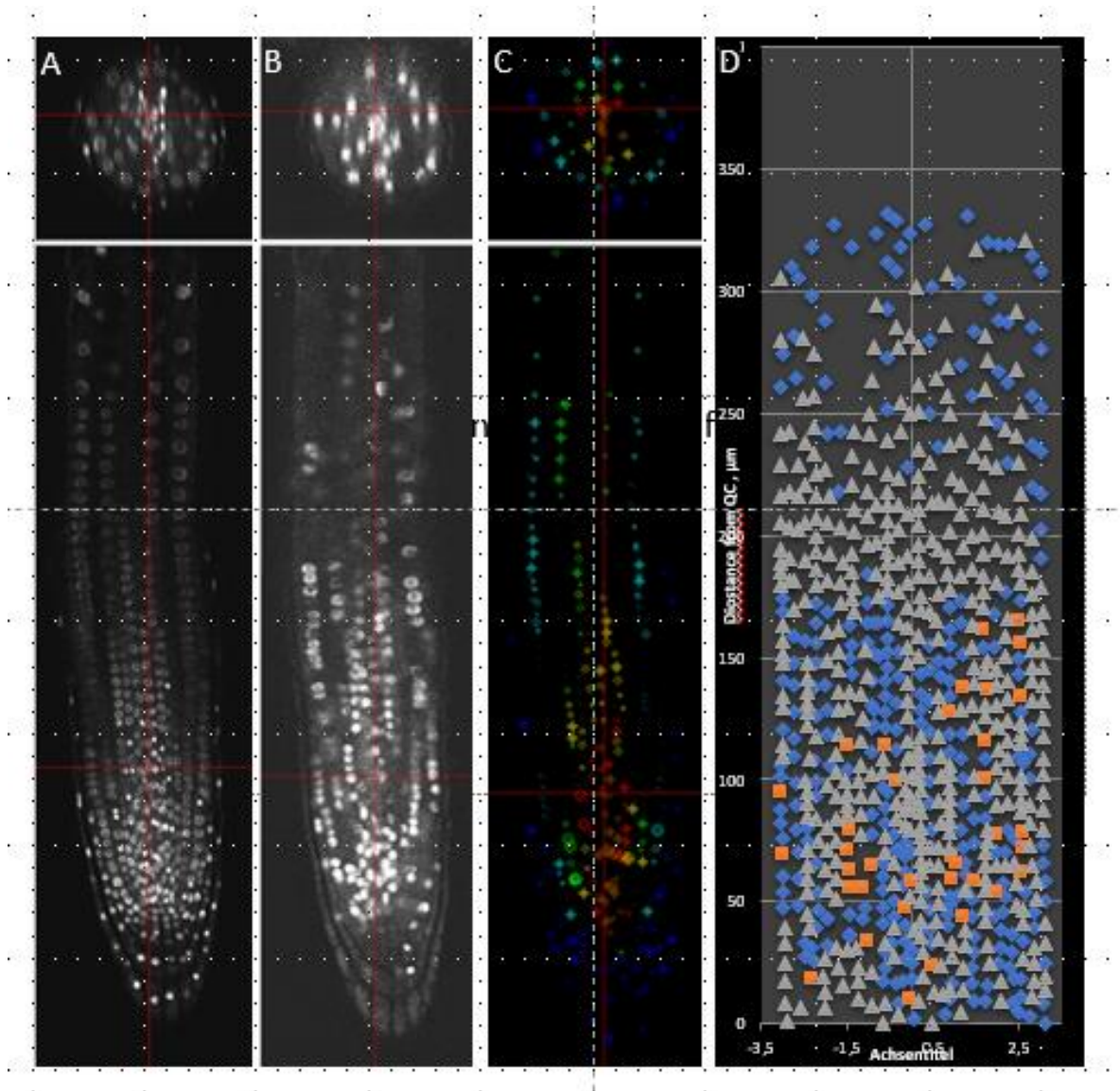
312 That's why determining the cell cycle kinetics and location are essential for understanding the
 313 mechanism of root growth. Root meristem consists of proliferation zone, transition zone, and

314 elongation zone. In proliferation zone occurred de novo cell production, while in the transition zone,
315 slight elongation accompanied by endocycle.

316 Detailed localization of all these parameters allows building functional root zonation (based on real
317 cell cycle and elongation kinetics). root zonation

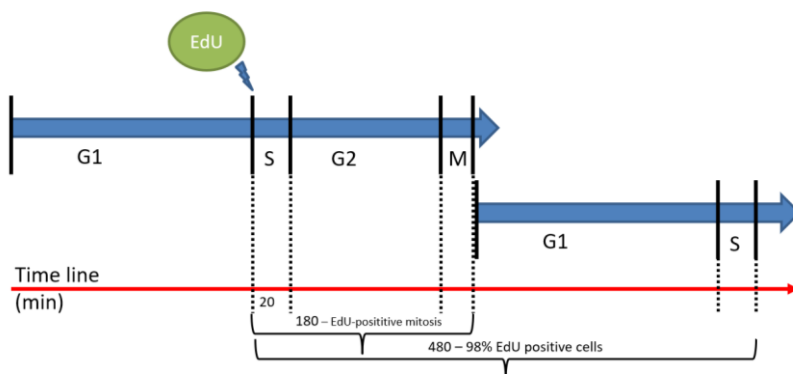
318 Figure 8 describes the example of functional root zonation in the epidermis of Arabidopsis root
319 (functional root zonation means root zonation) based on real cell cycle events, contrary to geometrical
320 2D root zonation based on cell length).

321 The cell cycle duration (how rapidly new cells are produced) is another key parameter determining the
322 kinetics of root growth. The platform also allows us to determine the kinetics of each stage of cell cycle
323 progression. Another feature is the determination of such mysterious events as stem cell division, and
324 it's distinguishing from an extension of stem cell niche by changes in post/mitotic cell fate. The rapid
325 divergence in the cell and nuclei volumes in different cell files starting from QC suggests differences in
326 chromatin structure which may cause differences in cell cycle progression. This led us to test our
327 workflow for analysis of the cell cycle of individual cells within each cell file and in each cell. We
328 demonstrated by using different EdU incubation times that our platform allows extraction of these data
329 (Pasternak et al., 2021). Briefly, S+G2 duration is depicted as the time proportional to abundance of for
330 EdU-positive and the whole cell cycle duration as the time required for EdU labeling of all cells. In
331 addition, a more prolonged time incubation with EdU (18–28 h) allows detection of quiescence levels
332 in the stem cell niche (Pasternak et al., 2021).



333
 334 **Figure 8.** Quantitative analysis of cell cycle kinetics in Arabidopsis root. A - DAPI; B - EdU; C - nucleus
 335 detection; D - analysis of the cell cycle events in the epidermis.

336
 337

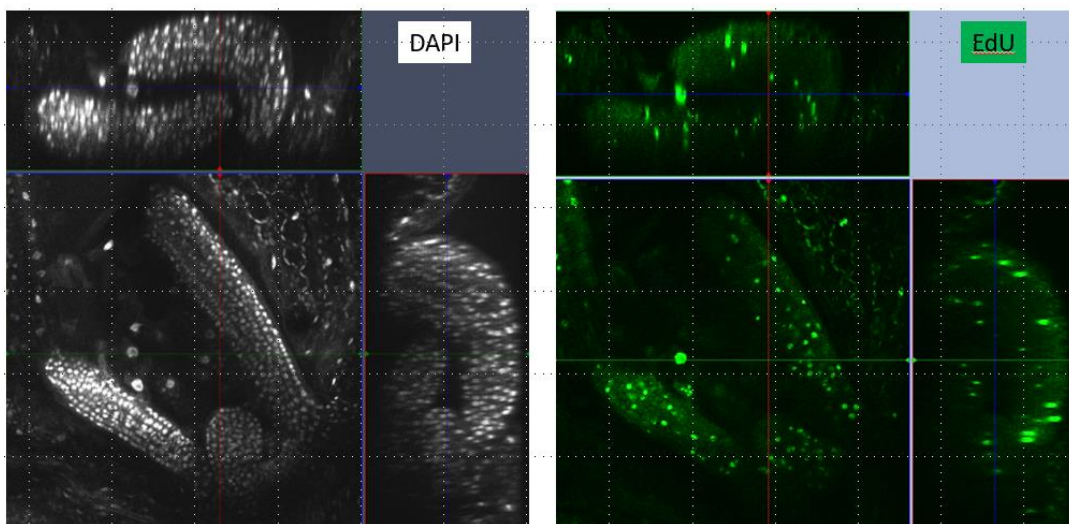


338
 339 **Figure 9.** Cell cycle duration analysis.

340 **Leaf/shoot functional analysis.**

341 Leaves and shoots represent rapidly developing organ(s) with a complicated structure that mostly
342 involves cell division orientation, cell polarity kinetics, and rapid divergence of cell fate. This platform
343 can quantify all these different features. Figure 10 shows an example of quantitative analysis of the cell
344 division orientation, PIN1 localization/polarity, and the induction of the first three leaves in 4-day-old
345 Arabidopsis seedlings. All nuclei were automatically detected, and the cell fate was labeled manually
346 (epidermis, mesophyll, and trichomes based on large nuclei and different orientations of the mitotic
347 plates). Application of the platform workflow allows also to analyze leaf zonation. In the leaf, the exit
348 from cell division starts from the leaf tip. In Arabidopsis leaves cells cease mitosis, but may continue
349 DNA replication to reach 8C/16C. Therefore, the leaf can also be divided into a “proliferation zone” and
350 a cell-type specific differentiating zone. The leaf has no mature zone (except several cells in the tips that
351 show very compact chromatin). Detailed maps of all of these events can be created.

352 In addition, mapping of the DNA replication events allows us to map endocycle in the mesophyll cells
353 of the cotyledon and quantify “ploidy level” after reduplication.



354 Figure 11.

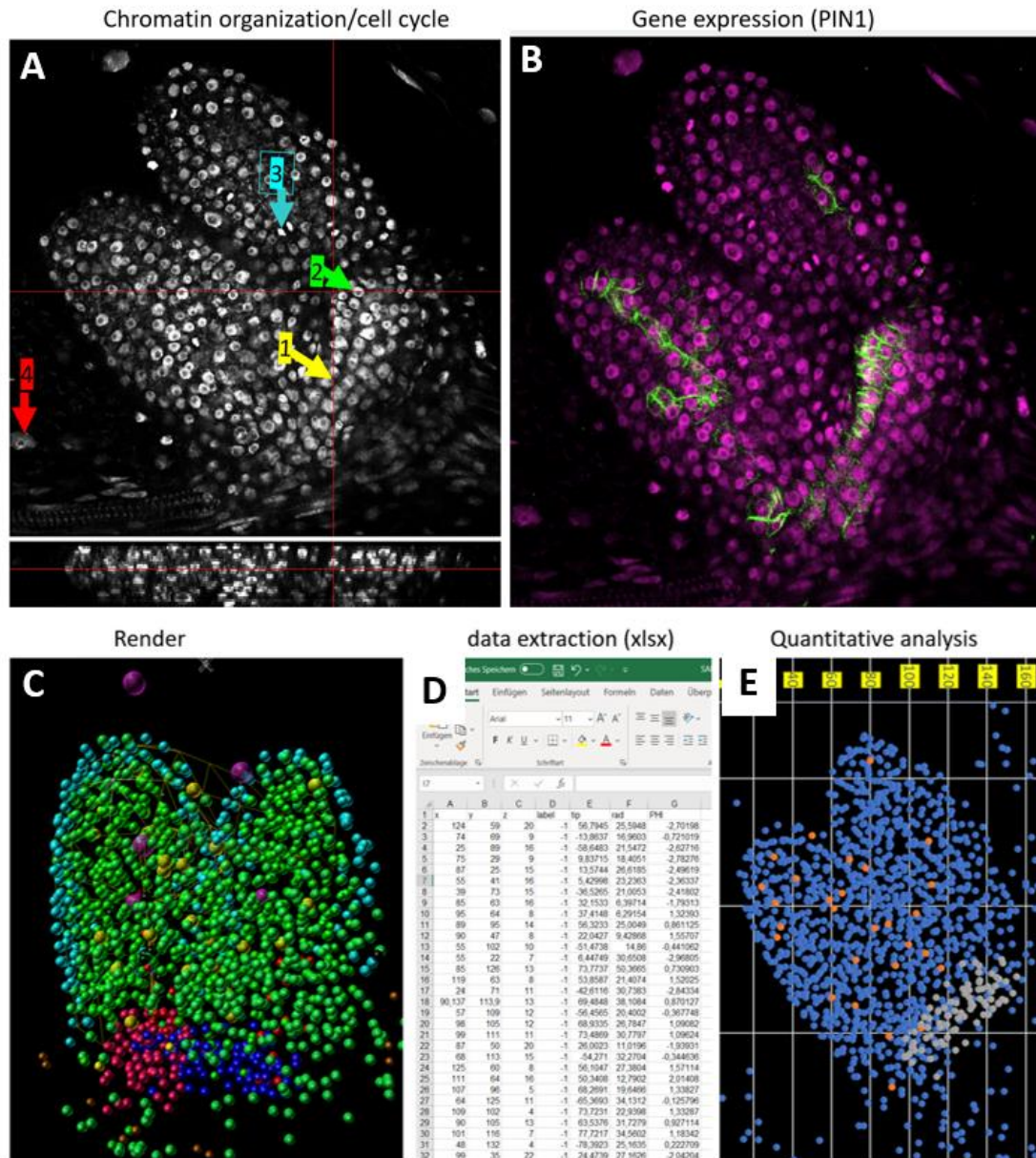
355 **Figure 11.** Analysis of cell cycle kinetics and endocycle in Arabidopsis shoot. Seedlings were incubated
356 with EdU for 45 minutes, fixed and EdU was detected with standard protocol. 3D
357 scanning/reconstruction were done.

358 **Analysis of the chromatin status.**

359 The chromatin structures in plants are determined by DNA methylation and histone modifications.
360 Chromatin organization contributes significantly to the regulation of the cell fate, cell cycle, and gene
361 expression. For this reason, we included in the platform options for quantifying different aspects of
362 epigenetic regulation *in situ* in the form of nucleus geometry (volume, nucleolus volume), histone
363 methylation, chromatin density, and chromosome numbers. One of the most visible markers of the cell
364 fate in Arabidopsis root is nuclear landscape (volume), which, in turn, is independent of chromosomes
365 number. Chromatin condensation is an added versatile marker of phloem cell fate (sieve elements)

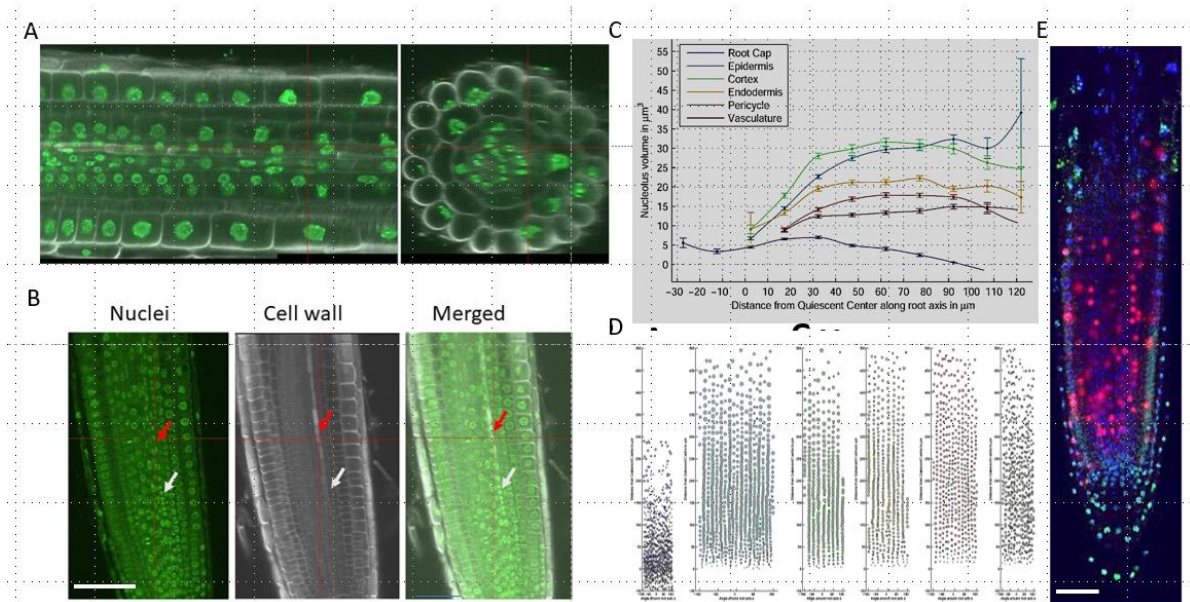
366 (panel (b)), as a heterochromatin map can be detected with a specific antibody. Examples of these
 367 options are presented in Figure 12.

368



369

370 **Figure 10.** Quantitative analysis of shoot apical meristem structure and leaf formation in 4-day-old
 371 Arabidopsis seedlings. The seedlings were fixed, subjected to PIN1 immunolocalization, co-staining
 372 with DAPI, 3D scanning, and image analysis. (A) DAPI stained 3D leaf image; (B) PIN1 localization;
 373 (C) rendering of the nuclei after detection; (D) quantitative extraction of cell position in relation to SAM
 374 as the center; Reconstruction of mitosis position in the SAM.



375

376

377 **Figure 12.** Chromatin analysis in Arabidopsis root.

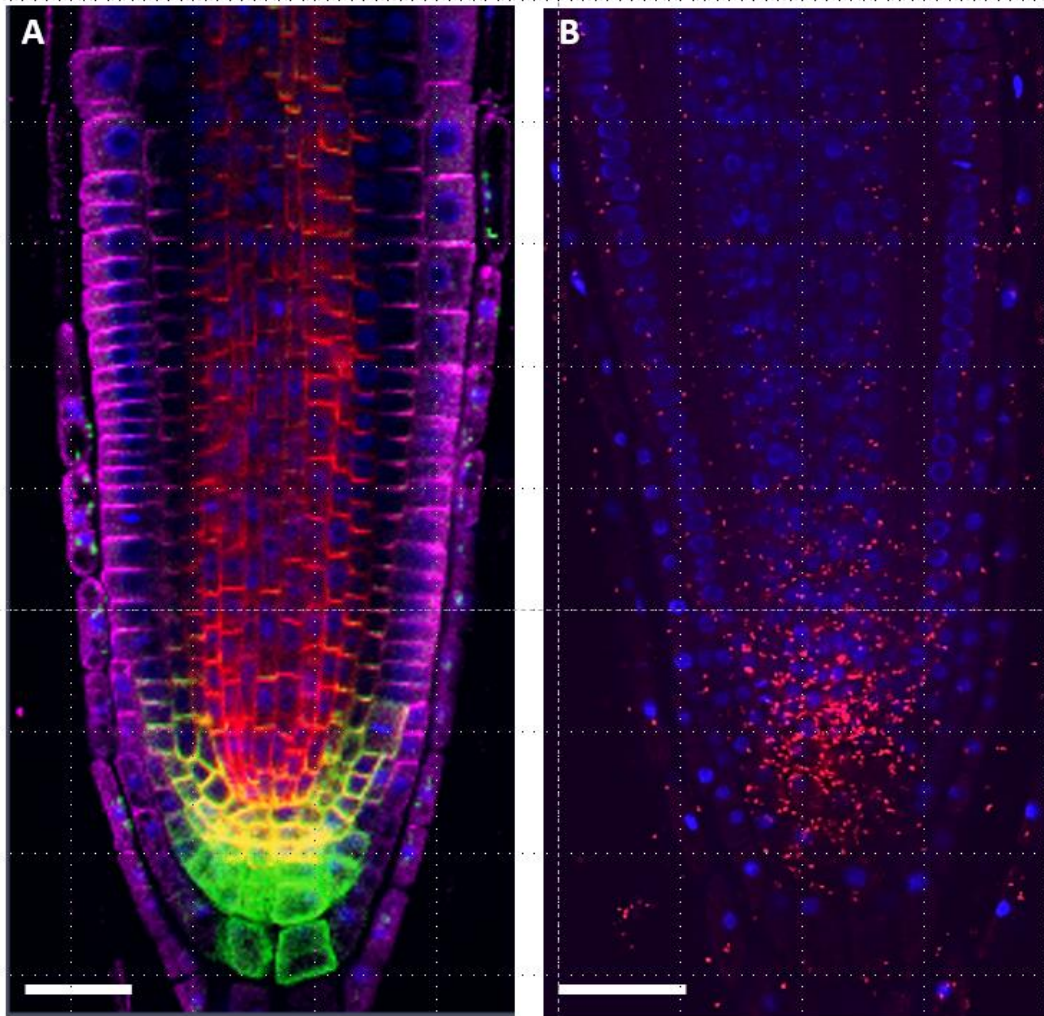
378 (A) cross-section of Arabidopsis root. Nuclei are indicated in green; cell borders are in white. The
 379 gradient in the chromatin landscape from the division to elongation zone is shown. Trichoblast (T);
 380 Cortex (C). The red arrow indicates condensed chromatin in the phloem. (B) chromatin condensation as
 381 a marker of phloem differentiation. The roots have been stained for nuclei (propidium iodide) and for
 382 cell walls (Calcofluor white). Cell differentiation in the phloem was detected as a decrease in nucleolus
 383 size and chromatin condensation (white arrow). (C) average nucleolus volume in different cell files at
 384 different distances from the quiescent center (QC). (D) distribution of nucleolus volume in the virtually
 385 unrolled root. The circle diameter is proportional to the nucleolus volume. (E) H3K9me2 localization
 386 (green) and EdU labeling (red) in Arabidopsis root. H3K9me2 is a marker of heterochromatin
 387 abundance.

388

389

390 **Protein localization and protein complex quantification *in situ*.**

391 Apart from monitoring the cell cycle, the platform can be used to monitor expression of individual
 392 protein as well as protein complexes using proximity for interactive labeling. Here the cell file-specific
 393 PIN1 localization is shown (Omelyanchuk et al., 2016) as well as complexes composed of different
 394 members of the PIN protein family (Pasternak et al., 2018). Quantitative analysis of proximity ligation
 395 assay (Pasternak et al., 2018) and demonstration of the mechanism of NPA action (; Teale et al.,
 396 2021).



397

398 **Figure 12.** Proximity ligation assay: detection of PIN1 and PIN4 complex in Arabidopsis root. (A) –
399 protein immunolocalization: PIN1 (red), PIN2 (magenta) and PIN4 (green) localization. (B) – Proximity
400 ligation assay (PLA): PIN1:PIN4 complex (red). Nuclei are indicated in blue; scale bar = 20 µm.

401

402 **Discussion**

403 Phenotyping has long been viewed as the main bottleneck in breeding programs; however, the main
404 focus of phenotyping was originally to characterize macroscopically the whole plant or plant organs
405 (Fiorani, F., & Schurr, U., 2013). This phenotyping helps to identify the relationship between genes and
406 complex traits, such as yield, plant height, root length, and root structure, but it does not help to
407 understand the processes occurring at the cellular level that guide plant growth and development.
408 Therefore, phenotyping at the cellular and subcellular levels, with the characterization of cell geometry
409 and function *in situ*, is a key tool for developing mechanistic models for understanding genotype–
410 environment interactions.

411 This phenotyping at the cellular and subcellular level can be attained by applying the DRPPP platform
412 to reconstruct different organs at high 3D-resolution. This platform has been successfully applied to
413 Arabidopsis and other plant species and explains their anatomical, morphogenetic, and functional traits.

414 The platform has four key parts that, in turn, represent different branches of science: plant growth (plant
415 biology), sample preparation (physic/chemistry), imaging (microscopy), and image analysis
416 (informatics). Only a combination of all these parts gives a satisfactory result. The preparation of
417 samples and image generations are the most important steps because excellent sample preparation avoids
418 many image analysis shortcomings.

419 We have described all the necessary details, from optimal growth conditions to the generation of the
420 high-resolution images (Pasternak et al., 2015; Pasternak et al., 2020). The main advantage of our
421 platform is that it is an endogenous marker-free system based on antibodies and other kinds of labeling.
422 Most of the currently available image analysis protocols are based on the use of endogenous marker
423 lines (see for example, Deshvoyes et al., 2020), which, on the one hand, have the advantages of saving
424 time and allow the use of living samples. However, on the other hand, they do not allow the use of any
425 mutants, especially if the mutants are in another genotypic background, and they do not allow the use
426 of commercial cultivars that do not have endogenous markers.

427 The image analysis toolbox is the fourth part of the platform. The main advantages of this toolbox are
428 the possibilities for simultaneous analysis of cell geometry, nuclei (cell cycle), and gene expression.
429 Apart from this segmentation/nucleus detection, the signal quantification, simple cell positioning (layers
430 recognition, cell position in organs, cell fate), and data extraction have primary importance. Our platform
431 automatically detects layers (based on the previous training model), automatically detects coordinate
432 systems, and automatically extracts all cell features using data conversion to a .csv file.

433 The platform has been applied thus far for the investigation of root zonation (Lavreha et al., 2017), new
434 WOX5 function in the Arabidopsis root (Savina et al., 2020), protein complex formation (Teale et al.,
435 2020), and cell cycle kinetics in *Nicotiana tabacum* root (Pasternak et al., 2017). With our platform,
436 precise single-cell phenotypes can be identified in their original tissue context, providing new
437 possibilities for direct *in situ* dissection of cell cycle kinetics and gene networks in the interaction with
438 neighboring cells/tissues.

439 The wide application of DRPPP motivates further development of its key parts, where development of
440 software for image analysis the most promising. Currently, in addition to iRoCS, the application of a
441 MorphoGraphX is also possible (de Reuille PB et al., 2015; Wolny, A., et al., 2020); however, this
442 software requires more computer resources and does not have a manual correction option. Moreover,
443 the MorphograhX was not used for nuclei detection and did not have an automatic coordinate system
444 for the root, and was not used for cell cycle detection.

445 During the development of DRPPP, we realized that only a few datasets were available to the plant
446 biologist community for training cell segmentation and cell cycle analysis tasks. We have addressed this
447 gap with a public release of sets of images and corresponding tutorials for each, as examples of
448 application of our platform.

449 **Author Contributions:** Conceptualization: KP, TP, TF, IP; methodology: TP, TF; Sample preparation,
450 scanning, image processing: TP; software develop: TF; data curation: TP, TF; writing IP, KP, TF. All
451 authors have read and agreed to the published version of the manuscript.

452

453 **Funding:** Experimental work was supported by Bundesministerium für Bildung und Forschung (BMBF
454 SYSBRA, SYSTEC, Microsystems), the Excellence Initiative of the German Federal and State
455 Governments (EXC 294), DFG (INST 39/839-1 FUGG), SFB746 and Deutsches Zentrum für Luft und
456 Raumfahrt (DLR 50WB1022).

457

458 **Acknowledgments:** to Franck Ditengou, Olaf Ronnenberger, Roland Nitschke and the staff of the Life
459 Imaging Center (LIC) in the Center for Biological Systems Analysis (ZBSA) of the Albert-Ludwigs-
460 University, Freiburg for help with their confocal microscopy resources, and the excellent support in
461 image recording.

462

463 **Conflicts of Interest:**

464 The authors declare no conflict of interest. The funders had no role in the design of the study; in the
465 collection, analyses, or interpretation of data; in the writing of the manuscript, or in the decision to
466 publish the results.

467

468 **Literature.**

469 **Bassel, G. W.** 2019. Multicellular systems biology: quantifying cellular patterning and function in plant
470 organs using network science. *Molecular Plant*. 12,6, 731-742.
471 DOI:<https://doi.org/10.1016/j.molp.2019.02.004>

472 **Desvoyes, B., Arana-Echarri, A., Barea, M. D., & Gutierrez, C.** 2020. A comprehensive fluorescent
473 sensor for spatiotemporal cell cycle analysis in Arabidopsis. *Nature Plants* 6, 1330-1334.

474

475 **Fiorani, F., & Schurr, U.** 2013. Future scenarios for plant phenotyping. *Annual Review Plant Biology*,
476 64, 267-291.

477

478 **Lavrekha, V. V., Pasternak, T., Ivanov, V. B., Palme, K., & Mironova, V. V.** 2017. 3D analysis of
479 mitosis distribution highlights the longitudinal zonation and diarch symmetry in proliferation activity
480 of the Arabidopsis thaliana root meristem. *The Plant Journal*, 92, 834-845.

481 **Liu, K., Schmidt, T., Blein, T., Dürr, J., Palme, K., & Ronneberger, O.** 2013 April Joint 3D cell
482 segmentation and classification in the Arabidopsis root using energy minimization and shape priors. In
483 2013 IEEE 10th International Symposium on Biomedical Imaging (pp. 422-425). IEEE.

484 **Liu, K., Lienkamp, S. S., Shindo, A., Wallingford, J. B., Walz, G., & Ronneberger, O.** 2014, April.
485 Optical flow guided cell segmentation and tracking in developing tissue. In 2014 IEEE 11th
486 International Symposium on Biomedical Imaging (ISBI) (pp. 298-301). IEEE.

487 **Omelyanchuk, N. A., Kovrizhnykh, V. V., Oshchepkova, E. A., Pasternak, T., Palme, K., &**
488 **Mironova, V. V.** 2016. A detailed expression map of the PIN1 auxin transporter in *Arabidopsis thaliana*
489 root. *BMC Plant Biology*, 16, 5.

490 **Pasternak, T., Tietz, O., Rapp, K., Begheldo, M., Nitschke, R., Ruperti, B., & Palme, K.** 2015.
491 Protocol: an improved and universal procedure for whole-mount immunolocalization in plants. *Plant*
492 *Methods*, 11, 50.

493 **Pasternak, T., Haser, T., Falk, T., Ronneberger, O., Palme, K., & Otten, L.** 2017. A 3D digital atlas
494 of the *Nicotiana tabacum* root tip and its use to investigate changes in the root apical meristem in-duced
495 by the *Agrobacterium* 6b oncogene. *Plant Journal*, 92(1), 31-42.

496 **Pasternak, T. P., Ruperti, B., & Palme, K.** 2020. A simple high efficiency and low cost in vitro growth
497 system for phenotypic characterization and seed propagation of *Arabidopsis thaliana*. *bioRxiv*.
498 <https://doi.org/10.1101/2020.08.23.263491>

499 **Pasternak, T., Teale, W., Falk, T., Ruperti, B., & Palme, K.** 2018. A PLA-iRoCS Pipeline for the
500 Localization of Protein–Protein Interactions In Situ. In *Phenotypic Screening* (pp. 161-170). Humana
501 Press, New York, NY.

502 **Pasternak, T. P., Kircher, S., & Palme, K.** 2021a. Estimation of cell cycle kinetics in higher plant root
503 meristem with cellular fate and positional resolution. *bioRxiv*, 2021-01.
504

505 **Pasternak, T., Paponov, I., Falk T.** 2021b. Deep-resolution plant phenotyping platform description..
506 [protocols.iohttps://dx.doi.org/10.17504/protocols.io.brsdm6a6](https://dx.doi.org/10.17504/protocols.io.brsdm6a6)
507

508 **Pearse Everson, A. G.** 1968. *Histochemistry, Theoretical and Applied*. Churchill, London, 439.

509 **de Reuille PB, Routier-Kierzkowska A-L, Kierzkowski D, Bassel GW, Schüpbach T, Tauriello G,**
510 **Bajpai N, Strauss S, Weber A, Kiss A.** 2015. MorphoGraphX: a platform for quantifying morphoge-
511 nesis in 4D. *eLife* 4: e05864.

512 **Rowland, R. E., & Nickless, E. M.** 2000. Confocal microscopy opens the door to 3-dimensional
513 analysis of cells. *Bioscene*, 26, 3-7.

514 **Savina, M. S., Pasternak, T., Omelyanchuk, N. A., Novikova, D. D., Palme, K., Mironova, V. V.,**
515 **& Lavrekha, V. V.** 2020 Cell dynamics in *WOX5*-overexpressing root tips: the impact of local auxin
516 biosynthesis. *Frontiers Plant Science*, 11.

517 **Schmidt, T., Pasternak, T., Liu, K., Blein, T., Aubry-Hivet, D., Dovzhenko, A., ... & Ronneberger,**
518 **O.** 2014. The iRoCS Toolbox–3D analysis of the plant root apical meristem at cellular resolution. *Plant*
519 *Journal*, 77, 806-814.

520 **Schulz, J., Schmidt, T., Ronneberger, O., Burkhardt, H., Pasternak, T., Dovzhenko, A., & Palme,**
521 **K.** 2006. Fast scalar and vectorial grayscale based invariant features for 3d cell nuclei localization and
522 classification. In *Joint Pattern Recognition Symposium* (pp. 182-191). Springer, Berlin, Heidelberg.

523 **Teale, W. D., Pasternak, T., Dal Bosco, C., Dovzhenko, A., Kratzat, K., Bildl, W., ... & Shahriari,**
524 **M.** (2020). Flavonol-mediated stabilization of PIN efflux complexes regulates polar auxin transport.
525 *The EMBO Journal*, e104416.

526 **Thompson, M. V., & Holbrook, N. M.** (2004). Root-gel interactions and the root waving behavior of
527 *Arabidopsis*. *Plant Physiology*, 135(3), 1822-1837.
528

529 **Truernit, E., Bauby, H., Dubreucq, B., Grandjean, O., Runions, J., Barthélémy, J., & Palauqui, J.**
530 **C.** 2008. High-resolution whole-mount imaging of three-dimensional tissue organization and gene
531 expression enables the study of phloem development and structure in Arabidopsis. *The Plant Cell* 20,
532 1494-1503.

533 **Wolny, A., Cerrone, L., Vijayan, A., Tofanelli, R., Barro, A. V., Louveaux, M., Wenzl C.,**
534 **Steigleder, S., Pape, C., Bailoni, A., Duran-Nebreda S., Bassel, G., Lohmann, J., Hamprecht, F.,**

535 **Schneitz, K., Maizel, A., Kreshuk A., & Duran-Nebreda, S.** 2020. Accurate and versatile 3D
536 segmentation of plant tissues at cellular resolution. *eLife* 2020;9:e57613 doi: 10.7554/eLife.57613